Transport properties of proton conductive Y-doped BaHfO and Ca or Sr-substituted Y-doped BaZrO

AUTHOR(S):

Kato, Kohei; Han, Donglin; Uda, Tetsuya

Transport Properties of Proton Conductive Y-Doped $BaHfO_3$ and Ca or Sr-Substituted Y-Doped $BaZrO_3$

Kohei Kato [a], Donglin Han [a *], and Tetsuya Uda [a *]

[a] Department of Materials Science and Engineering, Kyoto University,

Yoshida Honmachi, Sakyo-ku, Kyoto 606-8501, Japan

* Corresponding authors: Donglin Han (han.donglin.8n@kyoto-u.ac.jp)

Tetsuya Uda (uda_lab@aqua.mtl.kyoto-u.ac.jp)

TEL: +81-75-753-5445, FAX: +81-75-753-5284

Abstract

An electrolyte in fuel cells requires not only high ionic conductivity, but also high transport numbers of ionic conduction. Although Y-doped $BaZrO_3$ is regarded to be the most promising candidate as the electrolyte in protonic ceramic fuel cells (PCFCs), significant hole conduction generates in wet oxygen at high temperatures. With the aim to increase the transport number of ionic conduction, in this work, Sr and Ca were introduced to partially substitute Ba in $BaZr_{0.8}Y_{0.2}O_{3-\delta}$. The results revealed that a single cubic perovskite phase was obtained for $Ba_{0.95}Ca_{0.05}Zr_{0.8}Y_{0.2}O_{3-\delta}$ and $Ba_{1-x}Sr_xZr_{0.8}Y_{0.2}O_{3-\delta}$ (x = 0.05, 0.10, 0.15, 0.20 or 0.40). However, replacing Ba with Sr resulted in almost no increase of the transport number of ionic conduction in wet oxygen atmosphere, but drastic decrease in proton conductivity at all replacement levels. In addition, $Ba_{0.95}Ca_{0.05}Zr_{0.8}Y_{0.2}O_{3-\delta}$ shows no meaningful change in the transport number of ionic conduction, compared with $BaZr_{0.8}Y_{0.2}O_{3-\delta}$. Incorporating Ca or Sr into the Ba-site of $BaZr_{0.8}Y_{0.2}O_{3-\delta}$ appears to impart no positive influence on electrochemical properties. These interesting results also indicate that the hole conductivity decreases with the decrease of proton conductivity, and will aid to consider the hole conduction mechanism. $BaHfO_3$ doped with 10 and 20 mol% Y was also prepared. A bimodal microstructure was observed for $BaHf_{0.9}Y_{0.1}O_{3-\delta}$, whereas $BaHf_{0.8}Y_{0.2}O_{3-\delta}$ shows uniform grain size after sintering at 1600 ^oC for 24 h. The transport numbers of ionic conduction and bulk conductivity in such Y-doped $BaHfO_3$ samples are close to those of $BaZrO_3$ doped with the same amount of Y.

Keywords: Proton conductor; Fuel cells; Transport number; Barium zirconate; Barium Hafnate

1. Introduction

Nowadays, protonic ceramic fuel cells (PCFCs) which use proton conductive oxides as electrolytes are attracting increasing attention, due to their availability to operate at intermediate temperature around 600 °C, and no dilution of fuels by byproducts of water. Referring to the candidate for electrolytes of PCFCs, Y-doped $BaZrO_3$ (BZY), especially $BaZr_{0.8}Y_{0.2}O_{3-\delta}$ (BZY20), is currently regarded as the most promising one, since it shows high proton conductivity in wet atmosphere [1-4] and significant chemical stability against CO_2 [1, 5]. Although the ionic (mainly protonic) transport number (t_{ion}) of BZY is almost unity in wet reducing atmosphere, it deviates obviously from unity by exposing to wet oxidizing atmosphere at the temperature higher than 500 °C, due to the generation of hole conduction [6, 7]. Since the hole conduction results in the formation of leakage current in the electrolyte during the operation, and thereby reduces the performance of PCFCs [8], it's extremely important to suppress the hole conduction in the wet oxidizing atmosphere.

A recent study from our group [7] reported that $BaZr_{0.9}Y_{0.1}O_{3-\delta}$ exhibited t_{ion} around 0.24 at 700 °C in wet oxygen (p_{H_2O} = 0.05 atm). At the same temperature, interestingly, Bao, *et al*. reported t_{ion} of $CaZr_{0.95}Y_{0.05}O_{3-\delta}$ close to unity [9], and Pérez-Coll, *et al*. reported t_{ion} of $SrZr_{0.9}Y_{0.1}O_{3-\delta}$ higher than 0.8 in wet oxidizing atmosphere [10], indicating the possibility to increase t_{ion} of BZY by substituting Ba partially with Sr or Ca. In addition, $BaZrO_3$ and $BaHfO_3$ were generally supposed to have analogous properties, since Hf and Zr belong to the same group in periodic table, and the radii of six-coordinated tetravalent Hf and Zr cations to occupy the B-site of perovskite-type structure (ABO_3) are very close;

that is, 0.71 and 0.72 Å, respectively. [11] But, as far as we know, there is no detailed study on the transport properties of Y-doped $BaHfO_3$. In this work, we report the preparation and transport properties of $Ba_{1-x}Sr_xZr_{0.8}Y_{0.2}O_{3-\delta}$, $Ba_{1-x}Ca_xZr_{0.8}Y_{0.2}O_{3-\delta}$, and $BaHfO_3$ doped with 10 or 20 mol% Y.

2. Experimental

2.1. Material preparation

$Ba_{1-x}Sr_xZr_{0.8}Y_{0.2}O_{3-\delta}$ (x = 0.05, 0.10, 0.15, 0.20, and 0.40), $Ba_{1-x}Ca_xZr_{0.8}Y_{0.2}O_{3-\delta}$ (x = 0.05, 0.10, and 0.20), $BaHf_{1-x}Y_xO_{3-\delta}$ (x = 0.1, 0.2) were prepared by conventional solid state reaction method. $CaZr_{0.9}Y_{0.1}O_{3-\delta}$, $SrZr_{0.9}Y_{0.1}O_{3-\delta}$, $BaZr_{0.9}Y_{0.1}O_{3-\delta}$ and $BaZr_{0.8}Y_{0.2}O_{3-\delta}$ were also prepared for comparison. Starting materials of $BaCO_3$ (Wako Pure Chemical Industries, Ltd., 99%), $SrCO_3$ (Wako Pure Chemical Industries, Ltd., 99.9%), ZrO_2 (Tosoh Corporation, 97.07%), Y_2O_3 (Shin-Etsu Chemical Co., Ltd., 97.86%), $CaCO_3$ (Nacalai Tesque Inc., 99.5%) and HfO_2 (Mitsuwa Chemicals Co., Ltd., 99.9%) are mixed at desired ratio and ball-milled for 50 h. The mixtures were then placed in aluminum crucibles and heat-treated at 1000 °C for 10 h. After ball-milling for 24 h, the mixtures were pelletized under 9.8 MPa and synthesized at 1300 °C for 10 h in aluminum crucibles. The pellets were subsequently pulverized and ball-milled for 50 h. Then, the samples were combined with a binder (NCB-166, DIC Corporation, Tokyo, Japan) and pelletized under 392 MPa. After heating at 600 °C for 8 h to remove the binder, the pellets were covered with sacrificial powder composed of the as-synthesized powder and 1 wt% $BaCO_3$, and sintered at 1600 °C for 24 h in pure oxygen atmosphere

for most samples. For $Ba_{1-x}Ca_xZr_{0.8}Y_{0.2}O_{3-\delta}$ (x = 0.05 and 0.10) and $CaZr_{0.9}Y_{0.1}O_{3-\delta}$, a shorter sintering time of 10 h was selected, since the sinterability was greatly improved by adding calcium, and we found that sintering at 1600 °C for 24 h resulted in the difficulty to separate the pellets from the sacrificial powder.

2.2. Characterization

Crystal structure was analyzed by X-ray diffraction (XRD) method using Cu $K\alpha$ radiation with X'Pert-ProMPD (PANalytical, Almelo, Netherland). Rietveld refinement was performed to determine lattice constants with a commercial software X'Pert HighScore Plus. Microstructure was observed by field emission-electron probe microanalysis (FE-EPMA) with JXA-8530F (JEOL, Tokyo, Japan). Chemical compositions were determined by inductively coupled plasma atomic emission spectroscopy (ICP-AES) with SPS3500 (Seiko Instruments Inc., Chiba, Japan).

Pt electrode was deposited onto both surfaces of the pellet-like samples by sputtering. Electrical conductivity was determined from analyzing A. C. impedance spectroscopy collected in the frequency range of 10 Hz – 7 MHz using a frequency response analyzer (Solartron SI1260, Solartron Analytical, UK) with an applied A. C. voltage of 100 mV in wet atmosphere (p_{H_2O} = 0.05 atm) of pure or Ar-diluted O_2 or H_2. The Arrhenius plots were obtained by analyzing the data collected through cooling the samples gradually at the rate of 0.2 $^oCmin^{-1}$ from 700 to 100 ^oC in wet H_2, after the conductivity was stabilized at 700 ^oC. Furthermore, transport number of ionic conduction in wet oxidizing

atmosphere (t_{ion}) was estimated by evaluating the dependence of electrical conductivity on partial pressure of oxygen (p_{O_2}). Electronic holes ($h^{\bullet}$) are generated in oxidizing atmosphere following Eq. (1), in which $O_O^{\times}$ and $V_O^{\bullet\bullet}$ are oxide ions and oxide ion vacancies expressed in Kröger-Vink notation. Because of an assumption of the relatively small carrier density of hole, relationship of total conductivity (σ_{total}), ionic conductivity (σ_{ion}), hole conductivity (σ_h) and p_{O_2} can be expressed by (2) [6, 7]. By fitting the dependence of electrical conductivity on p_{O_2}, one can obtain the value of σ_{ion} and σ_h, leading to the determination of t_{ion} following Eq. (3).

$$2V_O^{\bullet\bullet} + O_2 = 2O_O^{\times} + 4h^{\bullet} \quad (1)$$

$$\sigma_{total} = \sigma_{ion} + \sigma_h (p_{O_2})^{\frac{1}{4}} \quad (2)$$

$$t_{ion} = \frac{\sigma_{ion}}{\sigma_{ion} + \sigma_h (p_{O_2})^{\frac{1}{4}}} \quad (3)$$

3. Results

3.1. Phase identification and Microstructure observation

(1) $Ba_{1-x}Sr_xZr_{0.8}Y_{0.2}O_{3-\delta}$ (x = 0.05, 0.10, 0.15, 0.20, 0.40)

The actual chemical compositions determined by ICP-AES measurements in general agree with the nominal value, as shown in **Table 1**. Powder XRD patterns of Sr-substituted $BaZr_{0.8}Y_{0.2}O_{3-\delta}$ after sintering at 1600 °C for 24 h in O_2 atmosphere are shown in **Fig. 1**. Only peaks belonging to a single cubic perovskite phase ($BaZrO_3$, JCPDS # 00-006-0399) were observed with the Sr content varying from 0 to 0.40. Then, the lattice constants were determined by simulating the XRD patterns using a

single cubic perovskite ($Pm\bar{3}m$) structure model [12, 13] with the Rietveld refinement, and plotted against the Sr content in **Fig. 2**. It is clear that the lattice constant decreases almost linearly with the increasing Sr content, following the Vegard's law due to the relatively smaller twelve-coordinated radius of divalent Sr cations (1.44 Å) than that of Ba cations (1.61 Å) [11]. From the microstructure shown in **Fig. 3**, one can see that with the Sr content increasing from 0 to 0.15, the grain size increases clearly. It was not obvious with Sr content over 0.2 because of a possible transcrystalline crack.

(2) $Ba_{1-x}Ca_xZr_{0.8}Y_{0.2}O_{3-\delta}$ (x = 0.05, 0.10, 0.20)

Powder XRD patterns of Ca-substituted $BaZr_{0.8}Y_{0.2}O_{3-\delta}$ are shown in **Fig. 4**. Only $Ba_{0.95}Ca_{0.05}Zr_{0.8}Y_{0.2}O_{3-\delta}$ appears to be a single perovskite phase. The lattice constant is about 4.214 Å, slightly smaller than that of $BaZr_{0.8}Y_{0.2}O_{3-\delta}$ (4.222 Å), since the twelve-coordinated radius of divalent Ca cations (1.34 Å) is smaller than that of Ba cations (1.61 Å) [11]. The grain size of $Ba_{0.95}Ca_{0.05}Zr_{0.8}Y_{0.2}O_{3-\delta}$, as shown in **Fig. 3(g)**, is about 1 μm. However, for the samples with the Ca content of 0.10 and 0.20, some small peaks belonging to second phase of Y_2O_3 appear. There are also two unknown peaks with negligibly low intensity rise at around 27.1 and 31.9 ^{o} in the XRD pattern of $Ba_{0.90}Ca_{0.10}Zr_{0.8}Y_{0.2}O_{3-\delta}$. These results indicate that the solid solubility of Ca into the Ba site should be smaller than 0.1.

(3) $BaHf_{1-x}Y_xO_{3-\delta}$ (x = 0.1 and 0.2)

Referring to Y-doped $BaHfO_3$, as shown in **Fig. 5**, only diffraction peaks belonging to perovskite phases ($BaHfO_3$, JCPDS # 00-024-0120) can be confirmed. However, from the insets of **Fig. 5**, in which the (211) diffraction peak was shown as an example, one can see that the (211) diffraction peak of $BaHf_{0.9}Y_{0.1}O_{3-\delta}$ is broad in shape, although the diffraction peak of $BaHf_{0.8}Y_{0.2}O_{3-\delta}$ is relatively sharp, and composed of two sub-peaks generated from Cu *K*α1 and Cu *K*α2 radiations. Microstructure shown in **Fig. 3(h)** and **(i)** indicates that the grain size of $BaHf_{0.8}Y_{0.2}O_{3-\delta}$ is relatively uniform with the size close to 1 μm, but the sample of $BaHf_{0.9}Y_{0.1}O_{3-\delta}$ appears to have a bimodal microstructure composed of large grains and fine grains, similar to the case of $BaZrO_3$ doped with 10 mol% rare earth elements, *e. g.*, Y and Tm [4, 14, 15, 16]. Our recent work revealed that these fine grains and large grains in such bimodal microstructure both have perovskite structures, but are different in the dopant content [4, 15]. Therefore, an analog case is supposed for $BaHf_{0.9}Y_{0.1}O_{3-\delta}$ here; that is, the fine and large grains might have different Y content.

3.2. Electrical conductivity

(1) $Ba_{1-x}Sr_xZr_{0.8}Y_{0.2}O_{3-\delta}$ (x = 0.05, 0.10, 0.15, 0.20)

The impedance spectra of $Ba_{0.80}Sr_{0.20}Zr_{0.8}Y_{0.2}O_{3-\delta}$ collected at 180 and 602 °C in wet H_2 atmosphere are plotted in **Fig. 6** for example to shown how the data were analyzed. At low temperature range, for example, at 180 °C, three semicircles appeared in the spectra, the ones at the high and middle

frequency ranges were determined to be attributed from the bulk (intra-grain) and grain boundary resistance, respectively, from their specific capacitance with the order of 10^{-9} and 10^{-11} F [17, 18], respectively. However, at high temperature range, for example, at 602 °C, only the semicircle of the grain boundary resistance can be qualitatively determined. In both the two cases, the total resistance, which is a sum of the bulk and grain boundary resistances, were determined from the intersect of the semicircles of the grain boundary resistance with the abscissa at the low frequency side. And the resistances of bulk and grain boundary are determined by reading the value at the valley between adjacent two semicircles, which is applicable typically at the temperature lower than 400 °C.

The Arrhenius plots of the electrical conductivity of Sr-substituted $BaZr_{0.8}Y_{0.2}O_{3-\delta}$ are shown in **Fig. 7**. It is clear the bulk, grain boundary and total conductivity tend to decrease with the increasing Sr content, except a slightly higher apparent grain boundary conductivity of $Ba_{0.90}Sr_{0.10}Zr_{0.8}Y_{0.2}O_{3-\delta}$ than $Ba_{0.95}Sr_{0.05}Zr_{0.8}Y_{0.2}O_{3-\delta}$. The results indicate a negative effect by introducing Sr into the Ba-site on the conductivity in the 20 mol% Y-doped system. Then, activation energy (E_a) and pre-exponential term (A) of the bulk conduction were evaluated by fitting the Arrhenius plots between 100 and 200 °C with Eq. (4), where k_b is Boltzmann's constant and T is temperature. The results are summarized in **Table 2**, showing that the activation energy increases as Sr content increases.

$$\sigma_{\text{bulk}}T = A\exp\left(\frac{-E_a}{k_b T}\right) \quad (4)$$

(2) $BaHf_{1-x}Y_xO_{3-\delta}$ (x = 0.1 and 0.2)

Fig. 8 shows the Arrhenius plots of the conductivity of Y-doped $BaHfO_3$ with those of Y-doped $BaZrO_3$ as reference. The bulk conductivity of Y-doped $BaHfO_3$ is close to that of Y-doped $BaZrO_3$ with the same Y-doping level. The activation energy and pre-exponential factor were also calculated, and listed in **Table 2**. Clearly, the bulk conductivity of $BaHf_{0.8}Y_{0.2}O_{3-\delta}$ is higher than that of $BaHf_{0.9}Y_{0.1}O_{3-\delta}$. One of the reasons is the increase in the oxide ion vacancies ($V_O^{\bullet\bullet}$) formed by replacing tetravalent Hf cations ($Hf_{Hf}^{\times}$) with trivalent Y cations ($Y_{Hf}^{'}$) following Eq. (5), which benefits the introduction of charge carriers of protons ($OH_O^{\cdot}$) through the hydration reaction (Eq. (6)). But the difference in bulk conductivity is more than twice and the activation energy is not equal. These fact means that samples with bimodal microstructure has lower proton mobility.

$$Y_2O_3 + 2Hf_{Hf}^{\times} + O_O^{\cdot\cdot} = 2Y_{Hf}^{'} + 2HfO_2 + V_O^{\cdot\cdot} \quad (5)$$

$$H_2O + V_O^{\cdot\cdot} + O_O^{\times} = 2OH_O^{\cdot} \quad (6)$$

As shown in **Fig. 8(b)**, the apparent grain boundary conductivity of $BaHf_{0.8}Y_{0.2}O_{3-\delta}$ is more than one order higher than that of $BaHf_{0.9}Y_{0.1}O_{3-\delta}$. In addition to the influence from defect chemistry suggested by Eq. (5) and (6), another major factor to the grain bograinundary conductivity is the difference in microstructure; that is, as aforementioned, $BaHf_{0.8}Y_{0.2}O_{3-\delta}$ has a relatively uniform but a little smaller grain size than $BaZr_{0.8}Y_{0.2}O_{3-\delta}$ (**Fig. 3(h) and (a)**), whereas $BaHf_{0.9}Y_{0.1}O_{3-\delta}$ shows a bimodal microstructure composed of large grains and fine grains(**Fig. 3(i)**). Fine grains drastically increase the area of grain boundary, thereby results in a decrease in apparent grain boundary conductivity. Since the apparent grain boundary conductivity is much lower than the bulk

conductivity, the total conductivity is mainly restricted by the low grain boundary conductivity as shown in **Fig. 8(c)**. And compared with Y-doped $BaZrO_3$, obviously lower grain boundary and total conductivities were confirmed in Y-doped $BaHfO_3$ doped with the same amount of Y.

3.3. Transport number of ionic conduction in wet oxygen

(1) 10 mol% Y-doped $CaZrO_3$, $SrZrO_3$ and $BaZrO_3$

According to literature [7, 9, 10], Y-doped $CaZrO_3$ or $SrZrO_3$ seems to show higher transport number of ionic conduction than Y-doped $BaZrO_3$ in wet oxidizing atmosphere. However, these data were collected on the samples containing different Y content, and the measurements were performed in atmosphere with different partial pressure of oxygen and water vapor. So preliminarily, it is necessary to check whether such conclusion is correct at the same Y-doping level under the same experimental condition.

The system with 20 mol% Y should be an optimal choice, but $SrZr_{0.8}Y_{0.2}O_{3-\delta}$ is not a single perovskite phase after sintering at 1600 ^{o}C in oxygen for 24 h (**Fig. S1(c)**). Here, 10 mol% Y-doped $CaZrO_3$, $SrZrO_3$ and $BaZrO_3$, which were of a single phase judged from XRD analysis (**Fig. S1**), were tested instead. It is worth to note that $BaZr_{0.9}Y_{0.1}O_{3-\delta}$ shows a bimodal microstructure similar with $BaHf_{0.9}Y_{0.1}O_{3-\delta}$, whereas $CaZr_{0.9}Y_{0.1}O_{3-\delta}$ and $SrZr_{0.9}Y_{0.1}O_{3-\delta}$ have grains with relative uniform size around 6 and 1 μm, respectively, estimated from EPMA second electron images (**Fig. S2**). The dependence of total conductivity, which is the sum of the partial conductivities of different charge

carriers (protons, oxide ions, holes, *etc*.) and also possibly dependent on microstructure, on partial pressure of oxygen were fitted using Eq. (2) (**Fig. S3**), and the thereby obtained σ_{ion} and σ_h were used to determine t_{ion} following Eq. (3) with the results listed in **Table 3**. Notably, the transport number of ionic conduction does increase in the sequence of $BaZr_{0.9}Y_{0.1}O_{3-\delta}$, $SrZr_{0.9}Y_{0.1}O_{3-\delta}$ and $CaZr_{0.9}Y_{0.1}O_{3-\delta}$. For example, the transport number of ionic conduction of $BaZr_{0.9}Y_{0.1}O_{3-\delta}$ is 0.28 at 700 °C, but increased to 0.67 and 0.85 for $SrZr_{0.9}Y_{0.1}O_{3-\delta}$ and $CaZr_{0.9}Y_{0.1}O_{3-\delta}$, respectively.

(2) $Ba_{1-x}Sr_xZr_{0.8}Y_{0.2}O_{3-\delta}$ (x = 0.05, 0.10, 0.15, 0.20, 0.40)

The dependence of total conductivity of Sr-substituted $BaZr_{0.8}Y_{0.2}O_{3-\delta}$ on partial pressure of oxygen was also fitted, as shown in **Fig. 9**, to determine the transport number of ionic conduction, which was summarized in **Table 3** and also plotted in **Fig. 10** with the total conductivity. One can see that the transport number of ionic conduction does not obviously increase with the increasing Sr content. Substituting Ba with 40 mol% Sr just results in the transport number elevating from 0.39 ($BaZr_{0.8}Y_{0.2}O_{3-\delta}$) to 0.41 ($Ba_{0.6}Sr_{0.4}Zr_{0.8}Y_{0.2}O_{3-\delta}$). However, the total conductivity decreases drastically with the increasing Sr content. When the Sr content is not larger than 0.1, the total conductivity is higher than 0.01 Scm^{-1}, meeting the requirements on ionic conductivity for the application as an electrolyte [19]. However, when the Sr content is increased to 0.15 and even larger, the total conductivity decreased below 0.01 Scm^{-1}.

(3) $Ba_{1-x}Ca_xZr_{0.8}Y_{0.2}O_{3-\delta}$ (x = 0.05) and $BaHf_{1-x}Y_xO_{3-\delta}$ (x = 0.1 and 0.2)

The transport number of ionic conduction in $Ba_{0.95}Ca_{0.05}Zr_{0.8}Y_{0.2}O_{3-\delta}$, the only sample of the single phase obtained for the Ca-substituted $BaZr_{0.8}Y_{0.2}O_{3-\delta}$ series in this work, and Y-doped $BaHfO_3$ were also measured and listed in **Table 3**. Similarly, substituting Ba with such small amount of Ca does not results in any meaningful change in the transport numbers. And the transport numbers of Y-doped $BaHfO_3$ are very close to those of the Y-doped $BaZrO_3$.

4. Discussion

A previous work of Bućko, *et al*. [20] reported an electrochemical study on $Ba_{1-x}Sr_xZr_{0.9}Y_{0.1}O_{3-\delta}$ with the Sr content varying from 0.03 to 0.1, and they found that substituting Ba with Sr enhanced the proton conduction. The Y content in their work is 0.1, and $BaZr_{0.9}Y_{0.1}O_{3-\delta}$ has a bimodal microstructure, which means that the total conductivity was predominated by the very low grain boundary conductivity [13, 14]. But, by introducing Sr into the Ba-site, the sinterability of $BaZr_{0.9}Y_{0.1}O_{3-\delta}$ was improved, resulting in reduction of the area of grain boundary. So, it might be the increase in grain boundary conductivity which directly elevates the total conductivity in such $Ba_{1-x}Sr_xZr_{0.9}Y_{0.1}O_{3-\delta}$ system. In this work, as shown in **Fig. 3**, the grain size of $BaZr_{0.8}Y_{0.2}O_{3-\delta}$ is uniformly around 2 μm, and substituting Ba with Sr with the amount up to 0.15 even increases the grain size. However, the bulk and apparent grain boundary conductivities both tend to decrease with the increasing Sr content. Such results indicate that although adding Sr with certain amount

beneficially improves the sinterability, Sr appears to have negative impact on the proton conduction. Doped with the same level of Y, $CaZrO_3$ and $SrZrO_3$ show higher transport number of ionic conduction than $BaZrO_3$. However, substituting Ba with Ca or Sr shows no meaningful effect on increasing the transport number of ionic conduction in $BaZr_{0.8}Y_{0.2}O_{3-\delta}$, but a large drop in proton conductivity was confirmed. The approximately fixed transport number of $Ba_{1-x}Sr_xZr_{0.9}Y_{0.1}O_{3-\delta}$ with the examined compositional range up to $x = 0.4$ indicates that the hole conductivity also decreases with the decrease of proton conductivity. However, the end member of Y-doped $SrZrO_3$ has the different and large transport number of ionic conduction. Explanation to this fact is difficult but one of the reasons might be due to crystal structure. The crystal structures of Y-doped $BaZrO_3$ and Y-doped $SrZrO_3$ are cubic and orthorhombic, respectively. Orthorhombic structure might be particularly unfavorable for hole conduction than hole conduction. It would be very interesting to study transport properties at the same composition with different virtual crystal structures by first principle calculation.

5. Conclusion

In this work, Ca and Sr were introduced into $BaZr_{0.8}Y_{0.2}O_{3-\delta}$ to partially substitute Ba. A single cubic perovskite phase was obtained for $Ba_{0.95}Ca_{0.05}Zr_{0.8}Y_{0.2}O_{3-\delta}$ and $Ba_{1-x}Sr_xZr_{0.8}Y_{0.2}O_{3-\delta}$ (x = 0.05, 0.10, 0.15, 0.20 or 0.40). Electrochemical analysis results revealed that substituting Ba with Sr resulted in almost no increase of the transport number of ionic conduction in wet oxygen atmosphere with the increasing Sr content. Furthermore, the proton conductivity in wet hydrogen atmosphere decreased

apparently with the increasing Sr. Similarly, no meaningful change in the transport number of ionic conduction was observed in $Ba_{0.95}Ca_{0.05}Zr_{0.8}Y_{0.2}O_{3-\delta}$ compared with $BaZr_{0.8}Y_{0.2}O_{3-\delta}$. Therefore, it can be concluded that incorporating Ca or Sr into the Ba-site of $BaZr_{0.8}Y_{0.2}O_{3-\delta}$ imparts no positive influence on electrochemical properties for the application as an electrolyte. $BaHfO_3$ doped with 10 and 20 mol% Y was also prepared. A bimodal microstructure was observed for $BaHf_{0.9}Y_{0.1}O_{3-\delta}$, whereas $BaHf_{0.8}Y_{0.2}O_{3-\delta}$ shows uniform grain size after sintering at 1600 ^{o}C for 24 h. The transport numbers of ionic conduction and bulk conductivity in such Y-doped $BaHfO_3$ samples are close to those of $BaZrO_3$ doped with the same amount of Y.

Acknowledgement

The authors want to thank Dr. Masatoshi Majima and Mr. Yohei Noda at Sumitomo Electric Industries, Ltd., for valuable discussion.

References

1. Kreuer KD. Proton-conducting oxides. Annu. Rev. Mater. Res. 2003; 33: 333-359.
2. Fabbri E, Pergolesi D, Licoccia S, Traversa E. Does the increase in Y-dopant concentration improve the proton conductivity of $BaZr_{1-x}Y_xO_{3-\delta}$ fuel cell electrolytes? Solid State Ionics. 2010; 181: 1043-1051.
3. Han D, Shinoda K, Sato S, Majima M, Uda T. Correlation between electroconductive and structural properties of proton conductive acceptor-doped barium zirconate. J. Mater. Chem. A, 2015; 3: 1243-1250.
4. Han D, Hatada N, Uda T. Chemical expansion of yttrium-doped barium zirconate and correlation with proton concentration and conductivity. J. Am. Ceram. Soc. 2016; 99: 3745-3753.
5. Fabbri E, D'Epifanio A, Bartolomeo ED, Licoccia S, Traversa E. Tailoring the chemical stability of $Ba(Ce_{0.8-x}Zr_x)Y_{0.2}O_{3-\delta}$ protonic conductors for intermediate temperature solid oxide fuel cells (IT-SOFCs). Solid State Ionics. 2008; 179: 558-564.
6. Nomura K, Kageyama H. Transport properties of $Ba(Zr_{0.8}Y_{0.2})O_{3-\delta}$ perovskite. Solid State Ionics. 2007; 178: 661-665.
7. Han D, Noda Y, Onishi T, Hatada N, Majima M, Uda T. Transport properties of acceptor-doped barium zirconate by electromotive force measurements. Int. J. Hydrogen Energy. 2016; 41: 14897-14907.
8. Nakamura T, Mizunuma S, Yamauchi K, Mikami Y, Kuroha T, Amezawa K. 18th International

Conference on Solid State Protonic Conductors, Oslo, Norway, 2016.

9. Bao J, Okuyama Y, Shin Z, Fukatsu N, Kurita N. Properties of Electrical Conductivity in Y-Doped $CaZrO_3$. Mater. Trans. 2012; 53: 973-979.
10. Pérez-Coll D, Heras-Juaristi G, Fagg DP, Mather GC. Transport-number determination of a protonic ceramic electrolyte membrane via electrode-polarisation correction with the Gorelov method. J. Power Sources. 2014; 245: 445-455.
11. Shannon RD, Revised effective ionic radii and systematic studies of interatomic distances in halides and chalcogenides. Acta Crystallogr. A. 1976; 32: 751-767.
12. Han D, Kishida K, Shinoda K, Inui H, Uda T. A comprehensive understanding of structure and site occupancy of Y in Y-doped $BaZrO_3$. J. Mater. Chem. A. 2013; 1: 3027-3033.
13. Han D, Shinoda K, Uda T,“Dopant site occupancy and chemical expansion in rare earth-doped barium zirconate. J. Am. Ceram. Soc. 2014; 97: 643-650.
14. Schober T, Bohn HG. Water vapor solubility and electrochemical characterization of the high temperature proton conductor $BaZr_{0.9}Y_{0.1}O_{2.95}$. Solid State Ionics. 2000; 127: 351-360.
15. Han D, Hatada N, Uda T. Microstructure, proton concentration and proton conductivity of barium zirconate doped with Ho, Er, Tm and Yb. J. Electrochem. Soc. 2016; 163: F470-F476.
16. Imashuku S, Uda T, Nose Y, Taniguchi G, Ito Y, Awakura Y. Dependence of dopant cations on microstructure and proton conductivity of barium zirconate. J. Electrochem. Soc. 2009; 156: B1-B8.

17. Haile SM, West DL, Campbell J. The role of microstructure and processing on the proton conducting properties of gadolinium-doped barium cerate. *J. Mater. Res*. 1998; 13: 1576-1595.

18. Han D, Nose Y, Shinoda K, Uda T. Site selectivity of dopants in $BaZr_{1-y}M_yO_{3-\delta}$ (M = Sc, Y, Sm, Eu, Dy) and measurement of their water contents and conductivities. *Solid State Ionics*. 2012; 213: 2-7.

19. Steele BCH, Heinzel A. Materials for fuel-cell technologies. *Nature*. 2001; 414: 345-352.

20. Bućko MM, Dudek M. Structural and electrical properties of $(Ba_{1-x}Sr_x)(Zr_{0.9}M_{0.1})O_3$, M = Y, La, solid solutions. *J. Power Sources*. 2009; 194: 25-30.

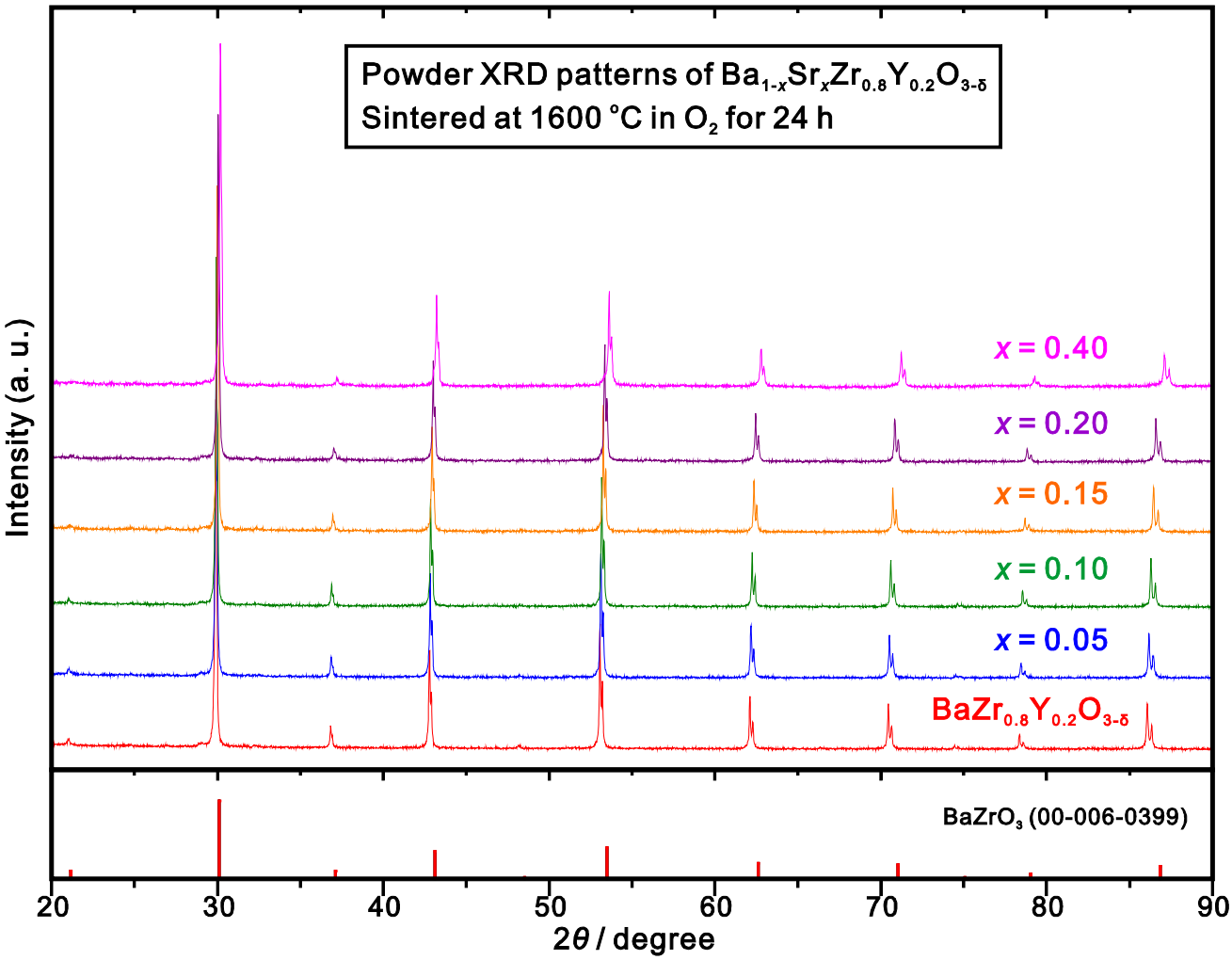

Fig. 1 Powder XRD patterns of $Ba_{1-x}Sr_xZr_{0.8}Y_{0.2}O_{3-\delta}$ (x = 0.05, 0.10, 0.15, 0.20, and 0.40) and $BaZr_{0.8}Y_{0.2}O_{3-\delta}$. The samples were sintered at 1600 °C in oxygen for 24 h.

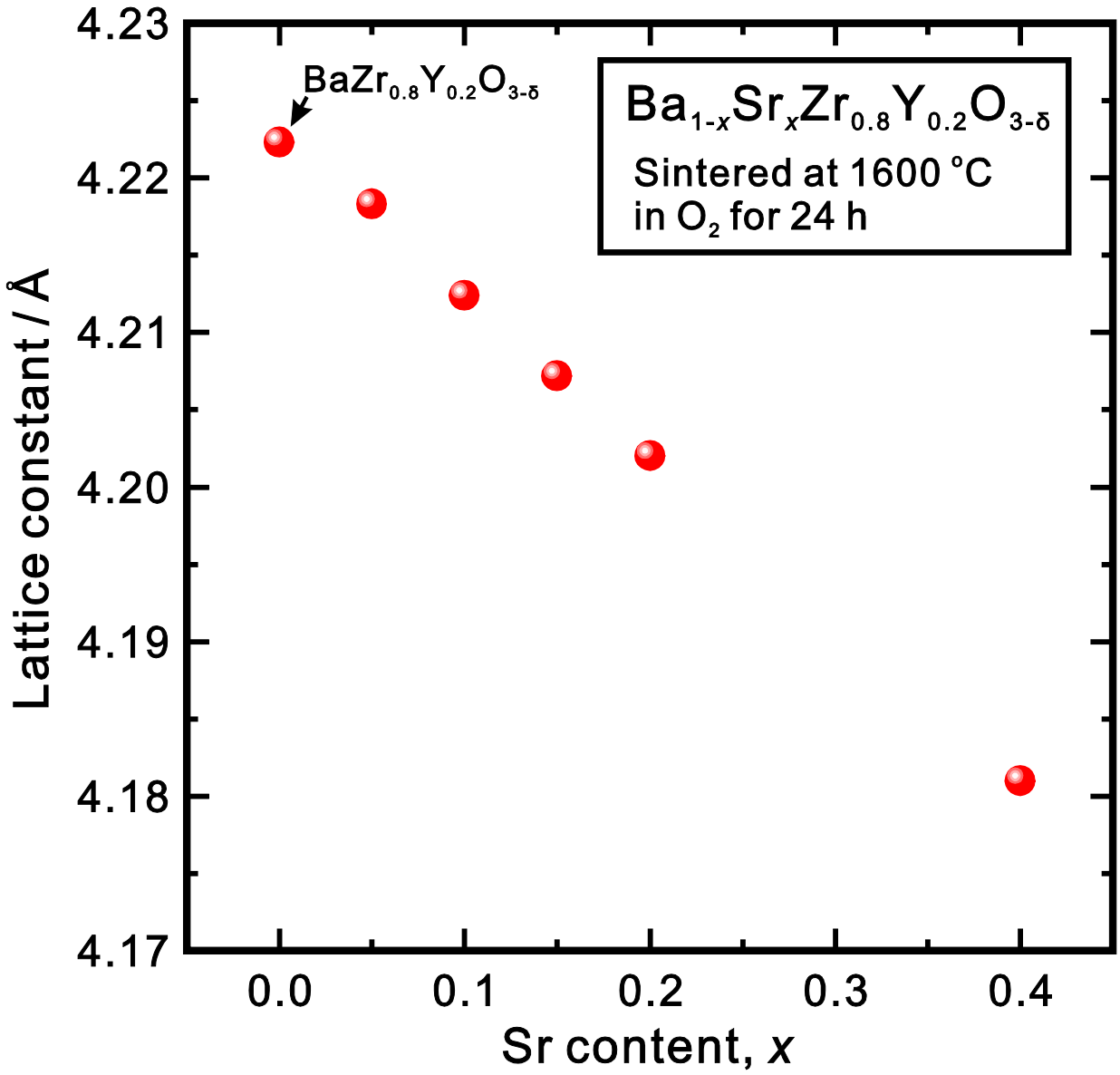

Fig. 2 Lattice constant of $Ba_{1-x}Sr_xZr_{0.8}Y_{0.2}O_{3-\delta}$ (x = 0, 0.05, 0.10, 0.15, 0.20, and 0.40). The samples were sintered at 1600 °C in oxygen for 24 h.

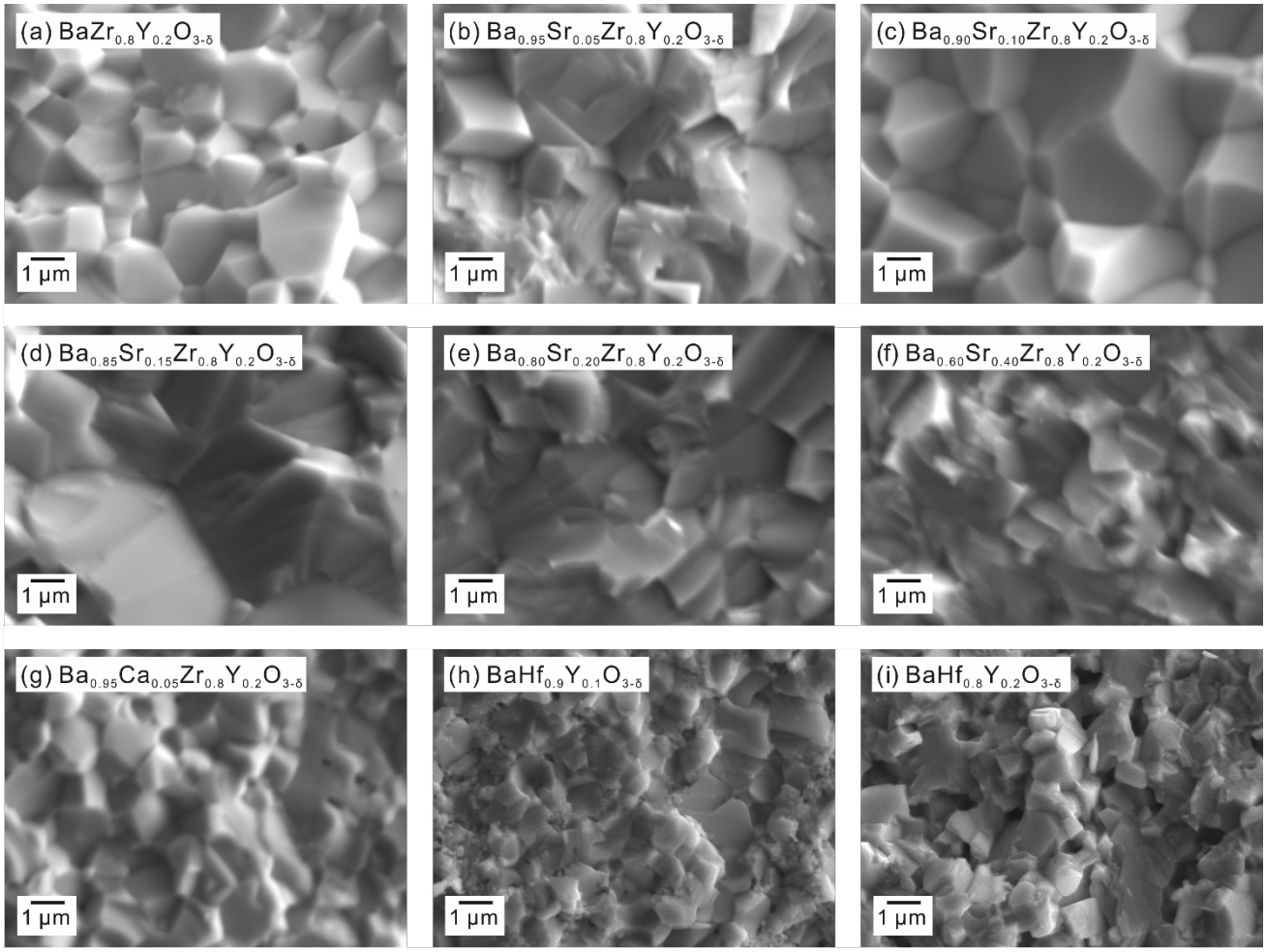

Fig. 3 EPMA second electron images of (a) $BaZr_{0.8}Y_{0.2}O_{3-\delta}$, (b) $Ba_{0.95}Sr_{0.05}Zr_{0.8}Y_{0.2}O_{3-\delta}$, (c) $Ba_{0.90}Sr_{0.10}Zr_{0.8}Y_{0.2}O_{3-\delta}$, (d) $Ba_{0.85}Sr_{0.15}Zr_{0.8}Y_{0.2}O_{3-\delta}$, (e) $Ba_{0.80}Sr_{0.20}Zr_{0.8}Y_{0.2}O_{3-\delta}$, (f) $Ba_{0.60}Sr_{0.40}Zr_{0.8}Y_{0.2}O_{3-\delta}$, (g) $Ba_{0.95}Ca_{0.05}Zr_{0.8}Y_{0.2}O_{3-\delta}$, (h) $BaHf_{0.9}Y_{0.1}O_{3-\delta}$ and (i) $BaHf_{0.8}Y_{0.2}O_{3-\delta}$. All the samples were sintered at 1600 °C in oxygen for 24 h, except $Ba_{0.95}Ca_{0.05}Zr_{0.8}Y_{0.2}O_{3-\delta}$ which was sintered at 1600 °C in oxygen for 10 h.

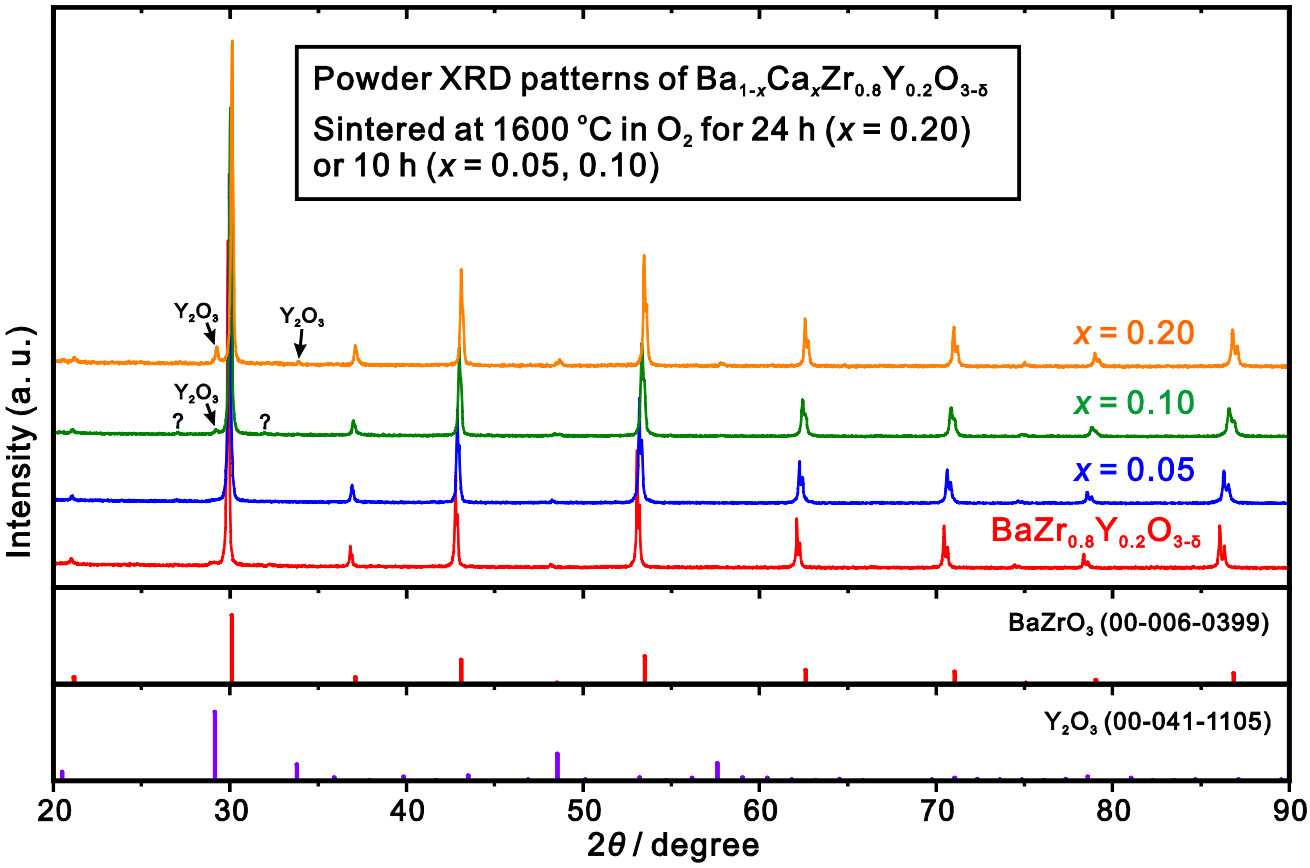

Fig. 4 Powder XRD patterns of $Ba_{1-x}Ca_xZr_{0.8}Y_{0.2}O_{3-\delta}$ (x = 0.05, 0.10, and 0.20) and $BaZr_{0.8}Y_{0.2}O_{3-\delta}$. The samples were sintered at 1600 °C in oxygen for 10 or 24 h. There are two unknown but very small peaks at the around 27.1 and 31.9 ° in the XRD pattern of $Ba_{0.9}Ca_{0.1}Zr_{0.8}Y_{0.2}O_{3-\delta}$.

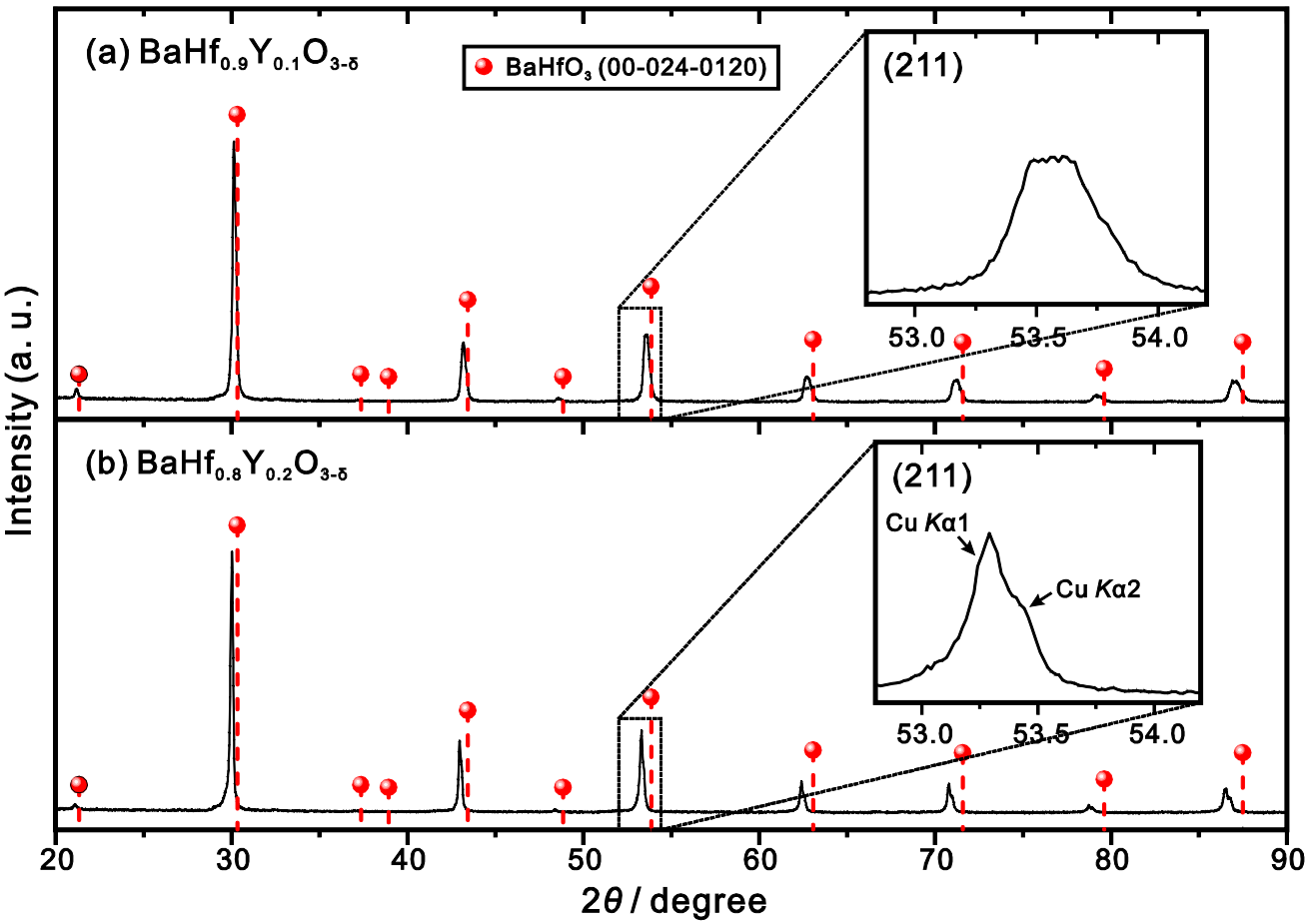

Fig. 5 Powder XRD patterns of $BaHf_{0.9}Y_{0.1}O_{3-\delta}$ and $BaHf_{0.8}Y_{0.2}O_{3-\delta}$, which were sintered at 1600 °C in oxygen for 24 h. The (211) diffraction peaks are magnified in insets to show the shape of peaks.

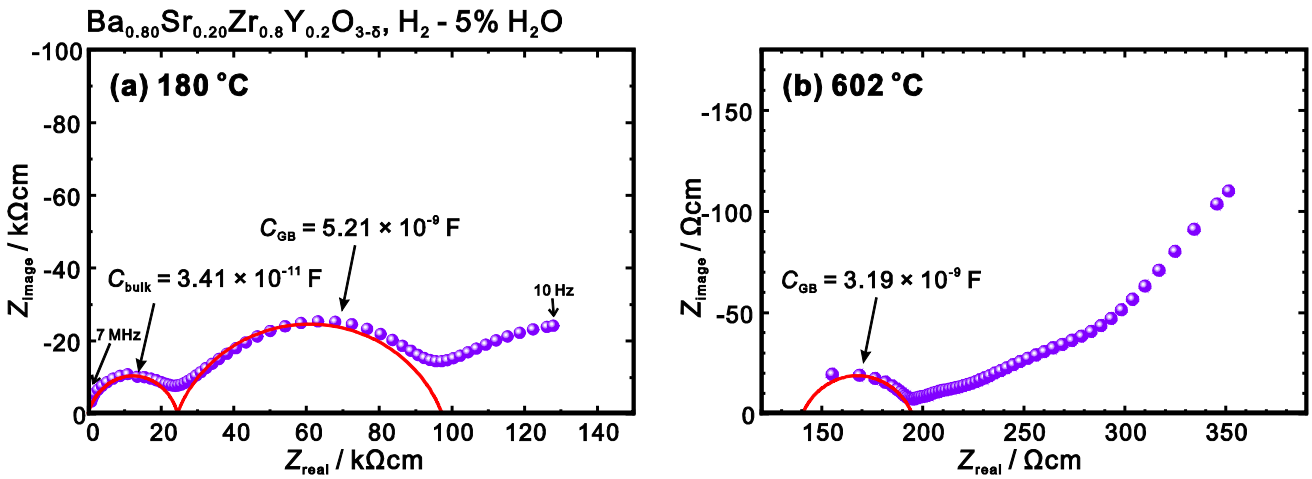

Fig. 6 Nyquist plots of of $Ba_{0.80}Sr_{0.20}Zr_{0.8}Y_{0.2}O_{3-\delta}$ collected at (a) 180.4 °C and (b) 602.2 °C in H_2 – 5% H_2O atmosphere. The identification of bulk and grain boundary (GB) were judged from their specific capacitance around 10^{-11} and 10^{-9} F, respectively.

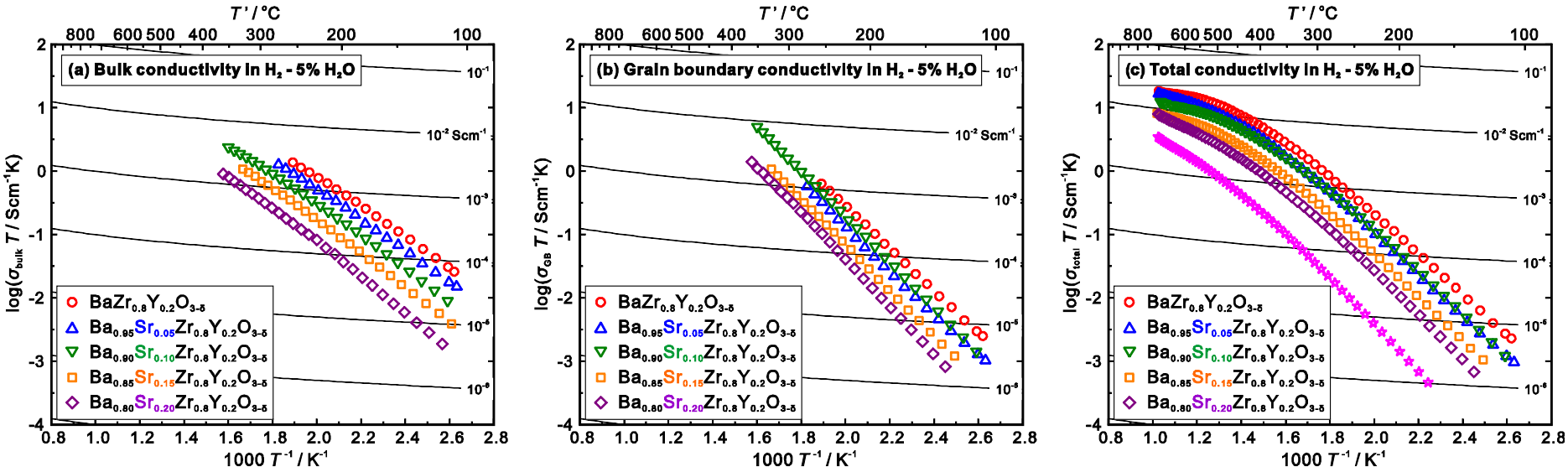

Fig. 7 Arrhenius plots of (a) bulk, (b) grain boundary, and (c) total conductivity of $Ba_{1-x}Sr_xZr_{0.8}Y_{0.2}O_{3-\delta}$ (x = 0.05, 0.10, 0.15, 0.20, and 0.40) and $BaZr_{0.8}Y_{0.2}O_{3-\delta}$ in H_2 - 5% H_2O atmosphere. All the samples were sintered at 1600 °C in oxygen for 24 h.

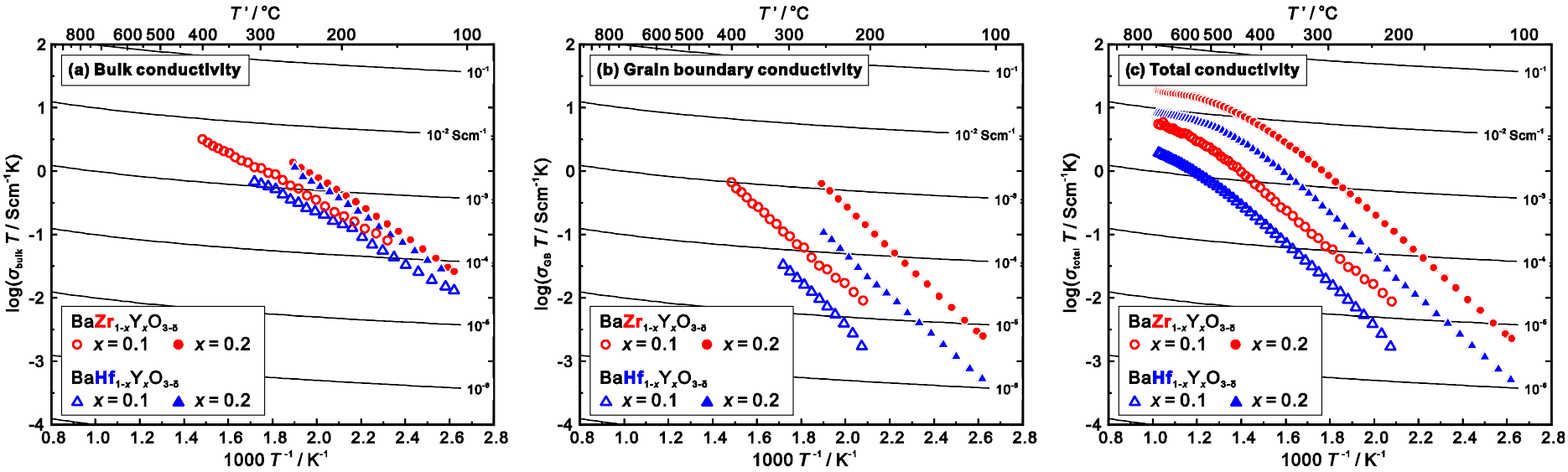

Fig. 8 Arrhenius plots of (a) bulk, (b) grain boundary, and (c) total conductivity of $BaHf_{1-x}Y_xO_{3-\delta}$ (x = 0.1 and 0.2) and $BaZr_{1-x}Y_xO_{3-\delta}$ (x = 0.1 and 0.2) in H_2 - 5% H_2O atmosphere. All the samples were sintered at 1600 °C in oxygen for 24 h.

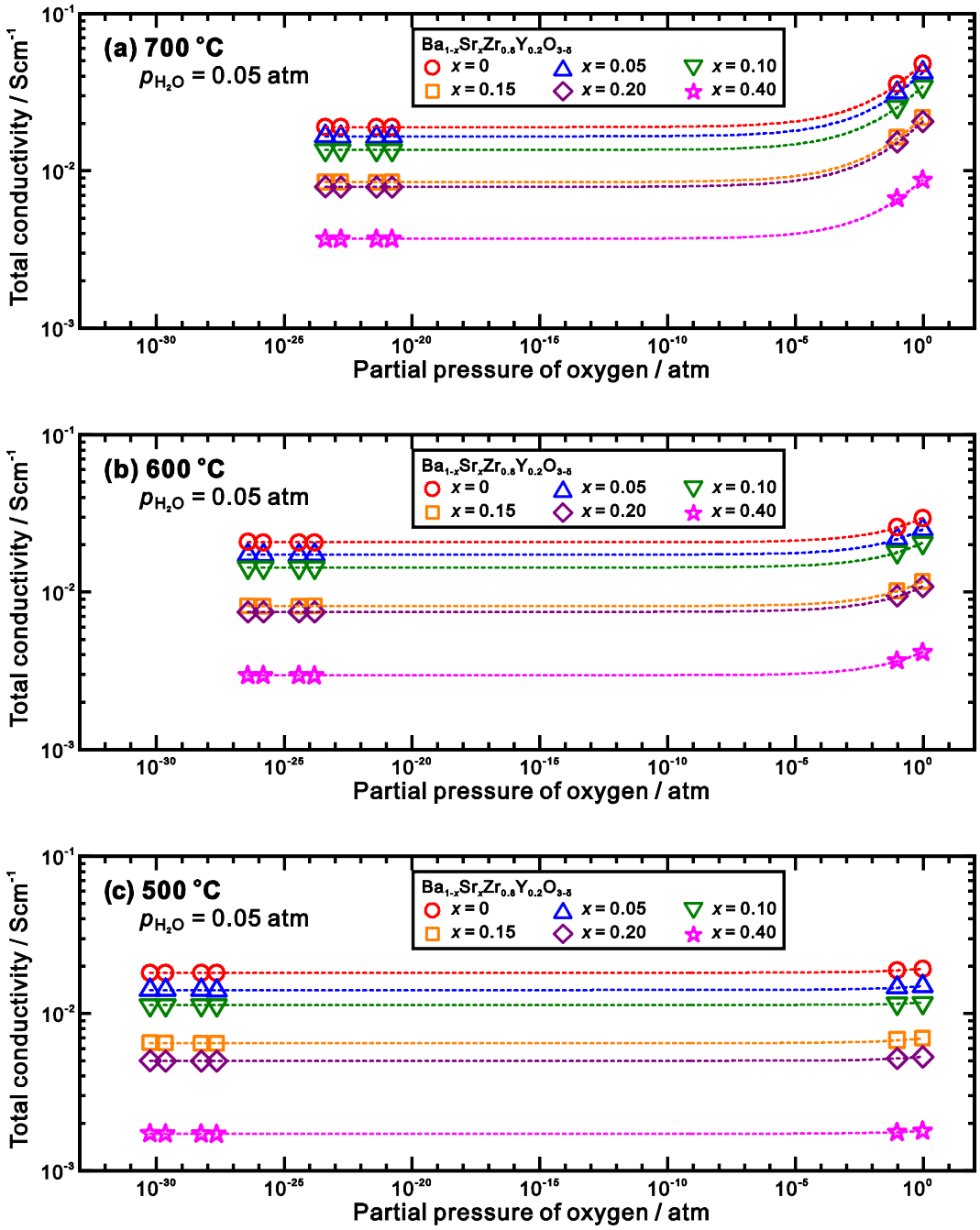

Fig. 9 Dependence of the total electrical conductivity on partial pressure of oxygen measured for $Ba_{1-x}Sr_xZr_{0.8}Y_{0.2}O_{3-\delta}$ (x = 0.05, 0.10, 0.15, 0.20, and 0.40) and $BaZr_{0.8}Y_{0.2}O_{3-\delta}$ at (a) 700 °C, (b) 600 °C and (c) 500 °C. All the samples were sintered at 1600 ºC in oxygen for 24 h.

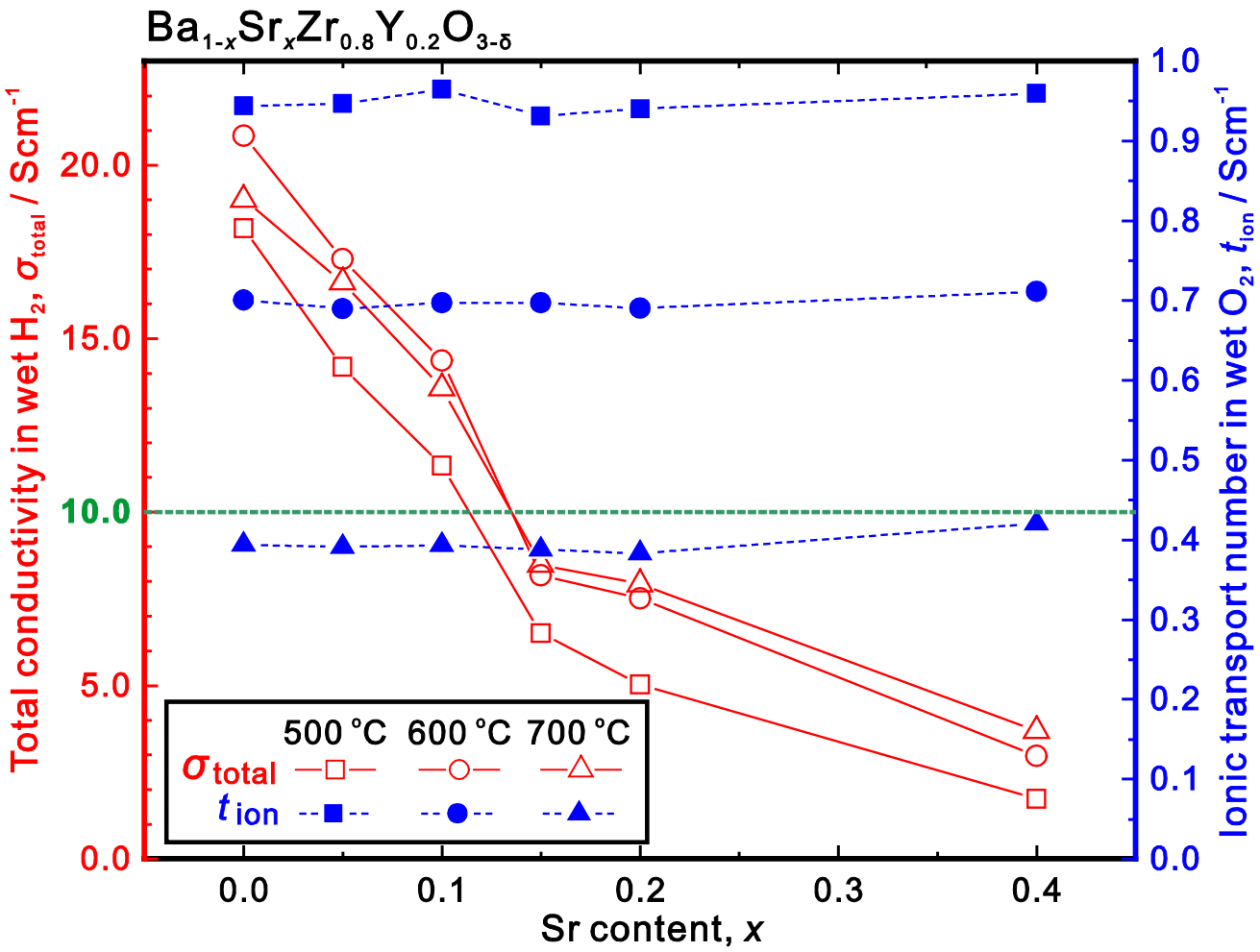

Fig. 10 Total electrical conductivity in wet H_2 (H_2 - 5% H_2O) and ionic transport number in wet O_2 (O_2-5%H_2O) measured at 500, 600 and 700 °C for $Ba_{1-x}Sr_xZr_{0.8}Y_{0.2}O_{3-\delta}$ (x = 0, 0.05, 0.10, 0.15, 0.20, and 0.40).

Table 1 Total compositions determined by ICP-AES of the samples prepared in this work.

Nominal composition	Composition determined by ICP-AES
$SrZr_{0.9}Y_{0.1}O_{3-\delta}$	$Sr_{1.02}Zr_{0.90}Y_{0.10}O_{3-\delta}$
$CaZr_{0.9}Y_{0.1}O_{3-\delta}$	$Ca_{1.04}Zr_{0.90}Y_{0.10}O_{3-\delta}$
$SrZr_{0.9}Y_{0.1}O_{3-\delta}$	$Sr_{1.02}Zr_{0.90}Y_{0.10}O_{3-\delta}$
$BaZr_{0.9}Y_{0.1}O_{3-\delta}$	$Ba_{1.00}Zr_{0.90}Y_{0.10}O_{3-\delta}$
$BaZr_{0.8}Y_{0.2}O_{3-\delta}$	$Ba_{1.01}Zr_{0.80}Y_{0.20}O_{3-\delta}$
$Ba_{0.95}Sr_{0.05}Zr_{0.8}Y_{0.2}O_{3-\delta}$	$Ba_{0.96}Sr_{0.05}Zr_{0.80}Y_{0.20}O_{3-\delta}$
$Ba_{0.90}Sr_{0.10}Zr_{0.8}Y_{0.2}O_{3-\delta}$	$Ba_{0.93}Sr_{0.10}Zr_{0.80}Y_{0.20}O_{3-\delta}$
$Ba_{0.85}Sr_{0.15}Zr_{0.8}Y_{0.2}O_{3-\delta}$	$Ba_{0.88}Sr_{0.15}Zr_{0.80}Y_{0.20}O_{3-\delta}$
$Ba_{0.80}Sr_{0.20}Zr_{0.8}Y_{0.2}O_{3-\delta}$	$Ba_{0.81}Sr_{0.20}Zr_{0.80}Y_{0.20}O_{3-\delta}$
$Ba_{0.60}Sr_{0.40}Zr_{0.8}Y_{0.2}O_{3-\delta}$	$Ba_{0.60}Sr_{0.39}Zr_{0.80}Y_{0.20}O_{3-\delta}$
$Ba_{0.95}Ca_{0.05}Zr_{0.8}Y_{0.2}O_{3-\delta}$	$Ba_{0.98}Ca_{0.05}Zr_{0.79}Y_{0.21}O_{3-\delta}$

Table 2 Activation energy (E_a) and pre-exponential term (A) of bulk conduction of $BaZr_{1-x}Y_xO_{3-\delta}$ (x = 0.1, 0.2), $Ba_{1-x}Sr_xZr_{0.8}Y_{0.2}O_{3-\delta}$ (x = 0, 0.05, 0.10, 0.15, and 0.20), and $BaHf_{1-x}Y_xO_{3-\delta}$ (x = 0.1, 0.2) measured in wet H_2 (H_2 - 5% H_2O). The data collected below 200 °C were used in fitting.

Composition	E_a / eV	A / Scm^{-1} K
$BaZr_{0.9}Y_{0.1}O_{3-\delta}$	0.383	2.40×10^3
$BaZr_{0.8}Y_{0.2}O_{3-\delta}$	0.488	7.27×10^4
$Ba_{0.95}Sr_{0.05}Zr_{0.8}Y_{0.2}O_{3-\delta}$	0.492	4.90×10^4
$Ba_{0.90}Sr_{0.10}Zr_{0.8}Y_{0.2}O_{3-\delta}$	0.525	6.46×10^4
$Ba_{0.85}Sr_{0.15}Zr_{0.8}Y_{0.2}O_{3-\delta}$	0.544	5.59×10^4
$Ba_{0.80}Sr_{0.20}Zr_{0.8}Y_{0.2}O_{3-\delta}$	0.575	5.22×10^4
$BaZr_{0.9}Hf_{0.1}O_{3-\delta}$	0.421	4.30×10^4
$BaZr_{0.8}Hf_{0.2}O_{3-\delta}$	0.483	4.78×10^4

Table 3 Transport number of ionic conduction (t_{ion}) in the samples prepared in this work in wet O_2 (O_2 – 5% H_2O) at 500, 600 and 700 °C. The samples were finally sintered at 1600 °C in oxygen.

Nominal Composition	t_{ion} in wet O_2			Nominal Composition	t_{ion} in wet O_2		
	500 °C	600 °C	700 °C		500 °C	600 °C	700 °C
$BaZr_{0.9}Y_{0.1}O_{3-\delta}$	0.89	0.60	0.28	$BaZr_{0.8}Y_{0.2}O_{3-\delta}$	0.94	0.70	0.39
$SrZr_{0.9}Y_{0.1}O_{3-\delta}$	1.02	0.90	0.67	$Ba_{0.95}Sr_{0.05}Zr_{0.8}Y_{0.2}O_{3-\delta}$	0.95	0.69	0.39
$CaZr_{0.9}Y_{0.1}O_{3-\delta}$	0.98	0.80	0.85	$Ba_{0.90}Sr_{0.10}Zr_{0.8}Y_{0.2}O_{3-\delta}$	0.96	0.70	0.39
$Ba_{0.95}Ca_{0.05}Zr_{0.8}Y_{0.2}O_{3-\delta}$	0.90	0.62	0.34	$Ba_{0.85}Sr_{0.15}Zr_{0.8}Y_{0.2}O_{3-\delta}$	0.93	0.70	0.39
$BaHf_{0.9}Y_{0.1}O_{3-\delta}$	0.88	0.60	0.34	$Ba_{0.80}Sr_{0.20}Zr_{0.8}Y_{0.2}O_{3-\delta}$	0.94	0.69	0.38
$BaHf_{0.8}Y_{0.2}O_{3-\delta}$	0.98	0.69	0.33	$Ba_{0.60}Sr_{0.40}Zr_{0.8}Y_{0.2}O_{3-\delta}$	0.96	0.71	0.42